

Flexibly Controlling the Polycrystallinity and Improving the Foaming Behavior of Polylactic Acid via Three Strategies

Wei Liu, Xian Wu, Xiaocheng Chen, Shan Liu, and Chun Zhang*

Cite This: *ACS Omega* 2022, 7, 6248–6260

Read Online

ACCESS |



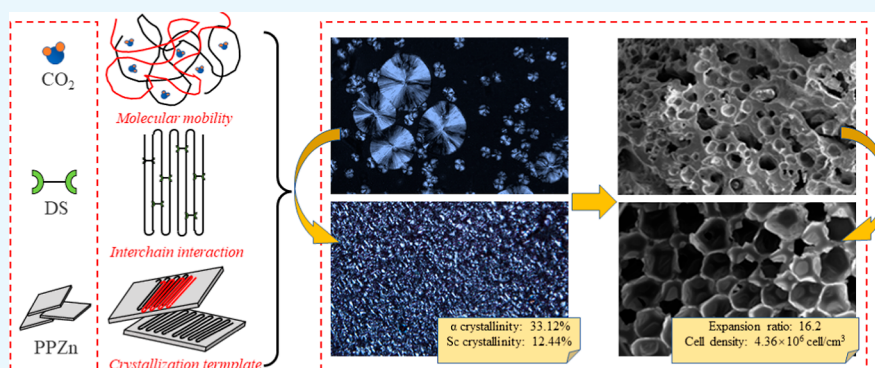
Metrics & More



Article Recommendations



Supporting Information



ABSTRACT: Controlling foamability plays the central role in preparing PLA foams with high performances. To achieve this, chain extension was often used to improve the rheological property of PLA resins; however, despite the availability of this approach, it often deteriorates the biodegradability of PLA and greatly increases the processing cost and complexity. Hence, we reported a special crystallization induction method to design PLA foams with a tunable cellular structure and a high expansion ratio. A novel crystallization-promoting agent combination (D-sorbitol, CO₂, and phenylphosphonic acid zinc salt) was used to induce PLA to enhance the chain interaction force and chain mobility and to provide crystallization templates. A series of PLAs with tunable stereocomplex (Sc)/ α crystallinity and rapid non-isothermal crystallization ability were obtained. The effect of various crystallization properties on the foaming behavior of PLA was studied. The results demonstrated that proper crystallization conditions (a small spherulite size, a crystallinity of 6%, and rapid crystallization ability) could virtually contribute to the optimized cellular structure with the highest cell density of 4.36×10^6 cell/cm³. When the Sc crystallinity was above 10%, PLA had a superior foamability, which thereby resulted in a high foaming expansion ratio of 16.2. A variety of cellular morphologies of PLA foams could be obtained by changing the foaming temperature and the crystallization property. The proposed crystallization-induced approach provided a useful method for controlling the cellular structure and the performances of the PLA foams.

1. INTRODUCTION

The past 2 decades had witnessed many efforts to precisely control and optimize the foaming process of PLA, especially via enhancing the melt strength. According to these efforts, PLA foams with special cellular structures, such as nanosize cells,¹ bimodal cells,² controllable open cells,³ and oriented cells,⁴ could be obtained. Besides, PLA foams with functional properties, such as electrical conductivity⁵ oil–water separation,⁶ as well as tissue scaffolding,⁷ could also be obtained. These works had provided many feasible strategies to produce biodegradable, high-performance, and versatile PLA foams.

In some cases, the foamability is the reflection of the viscoelastic property of the PLA resin. However, one of the unavoidable problems is that PLA had a nature of poor melt strength in the foaming process, which resulted in a narrow processing window and made it hard to obtain an ideal cellular structure. In order to solve this problem, several practical approaches continue to develop to increase the melt strength

of PLA through the chain extension technology^{8,9} or blending technology.^{10,11} According to these technologies, PLA chains would react with multifunctional compounds, such as triallyl isocyanurate (TAIC), pentaerythritol triacrylate (PETA), or trimethylolpropane trimethacrylate (TMPTA), and effectively enhance the melt strength and the resultant foamability. Driven by the significance of the chain-extension method, a question arises: is achieving better foamability of PLA as simple as creating a higher branching degree or cross-linking degree? The answer to the question is that it brought problems such as

Received: November 30, 2021

Accepted: January 27, 2022

Published: February 9, 2022



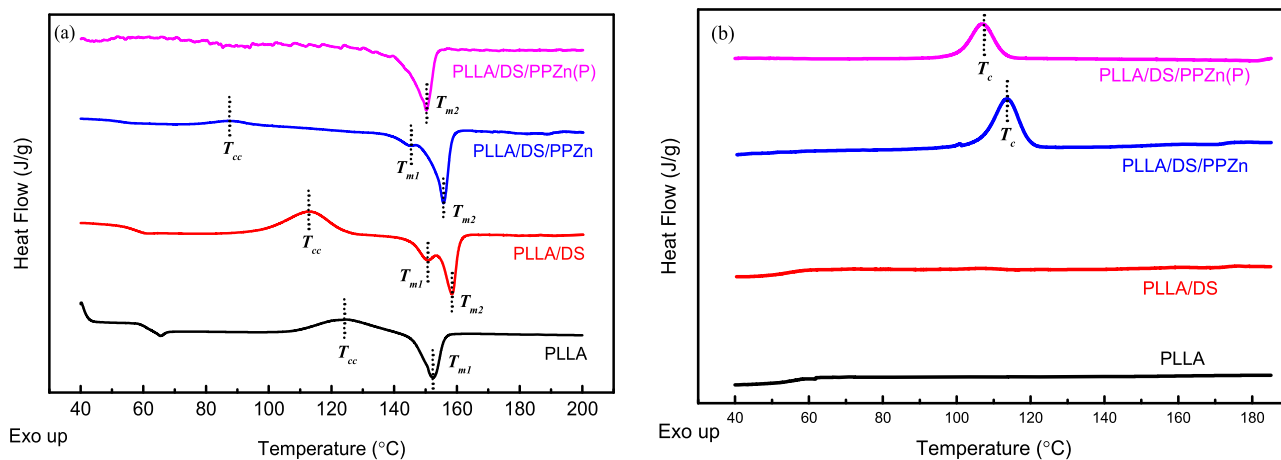


Figure 1. DSC curves of the PLLA blends with (a) a heating rate of 10 °C/min and (b) a cooling rate of 10 °C/min under atmospheric and high-pressure conditions.

a high cost, a two-step process, and an over-cross-linking degree, which hampered the processability and biodegradability at the beginning.

The key factor to improve the foamability of PLA is generating a suitable melt strength at the set foaming temperature. According to the classical foaming theory, a high melt strength value was associated with the extra resistance of cell growth, whereas a low melt strength value led to cell coalescence and rupture in the foaming process.¹² Many research works have revealed that increasing the melt strength of PLA could significantly facilitate the control of the cellular structure of PLA foams.^{13,14} It provided possible conditions for increasing PLA's melt strength without using a chain extender. It is well known that PLA is a kind of semicrystalline polymer.¹⁵ The presence of crystals could greatly increase the mechanical properties and thermal stability of PLA. However, crystals also affect the foaming behavior of PLA. In detail, the crystalline zone of PLA could influence foaming in two aspects. First, a foaming gas could not diffuse and dissolve into the crystalline zone in the gas saturation period. Hence, the solubility and the diffusivity of a foaming gas were related to the crystallinity of PLA,¹⁶ in which the crystalline zone could not be foamed due to the non-mobile nature of chains in the crystalline lattice.⁸ Therefore, the presence of abundant crystalline zones is expected to be detrimental to forming a fine cellular morphology in PLA foams and a narrow foaming process window. Second, the diffusion of a foaming gas only occurred in the amorphous zone, while crystalline zones could act as obstacles for a diffusing gas.¹⁷ The foaming gas molecules had to tortuously go around the crystallites, which relieved the escape of the foaming gas. Third, the small crystalline zones dispersed in the amorphous matrix could effectively restrict the thermal movement of molecular chains by physically entangling with chains around the crystallites. The crystals acted as physical network points, facilitating the improvement of the melt strength of PLA, which was favorable for the foaming process.²⁸ Based on the above reasons, it is believed that the foamability of PLA could be controlled by designing a proper crystalline structure and crystallinity. After that, PLA foams with a high expansion ratio and a high cell density without using the chain modification technology are expected to be obtained.

For the purpose of increasing the foamability by inducing crystallization, the crystallization of PLA should be understood. In PLA's crystallization process, the chains folded into different structural conformations and developed various crystals. The common crystal forms of PLA were α crystals and α' crystals.¹⁵ The melt temperature of α and α' crystals was 140–160 °C, which was close to the foaming temperature. However, the melt temperature (210 °C) of the stereocomplex (Sc) crystals was much higher than the foaming temperature. The Sc crystals could not be melted and remained intact due to their unusual high melt temperature; therefore, it is feasible to utilize Sc crystals to control the foaming behavior. However, the formation mechanisms and the promoting strategies for various crystal forms of PLA are different. Besides that, PLA chains are usually considered to lack in flexibility, and their conformation-changing ability is also weak. Therefore, PLA chains are difficult to move into the lattice space. Especially, in the case of non-isothermal crystallization conditions, there is not enough time for PLA chain rearrangement into the lattice, leading to the formation of an amorphous state. Hence, the addition of traditional inorganic nucleation agents, such as talc, zinc oxide, clay, and so forth, could not effectively induce high crystallinity or various crystal forms of PLA because they simply supplied crystallization nucleation sites.^{18–20} The use of some nucleation agents is that they easily decrease the molecular weight of PLA and deteriorate the foamability as well as the final mechanical properties of PLA. In order to better control various crystalline forms in PLA, both the interaction force between molecular chains and the chain mobility should be improved. In addition, crystalline templates should be supplied in a crystallization process. Meanwhile, as one of the important factors, the contribution of the crystalline form and the quantitative crystallization parameters to the foaming behavior of PLA should be studied and understood.

To solve this problem, a novel crystallization-promoting agent combination, namely D-sorbitol (DS), phenylphosphonic acid zinc salt (PPZn), and high-pressure CO₂, was used to simultaneously improve PLA chains' interaction force and chain mobility and to supply crystalline templates in this work. A series of PLAs that could rapidly crystallize even under non-isothermal conditions were achieved. The effect of quantitative crystallinity, crystallization rate, and crystalline morphology of PLA on appropriately controlling the foaming behavior was studied. The relationship between the crystal-

Table 1. Thermal Property Parameters of the PLLA Blends under Heating Conditions

sample	$T_{cc}/^{\circ}\text{C}$	J_{cc}/g	$T_m/^{\circ}\text{C}$	J_m/g	$X_c/\%$	$T_c/^{\circ}\text{C}$
PLLA	126.4	19.44	152.4	21.01	1.67	
PLLA/DS	112.7	22.55	158.5	29.31	7.29	
PLLA/DS/PPZn	87.4	3.28	155.7	33.71	33.12	113.5
PLLA/DS/PPZn(P)			150.3	26.96	29.35	106.9

lization property and the cell formation mechanism was discussed. The study of the tunable crystallization property is expected to provide a green method for the production of high-performance and biodegradable PLA foams without using a chain-extension method. This strategy also provides technological reference for designing similar crystalline polymer foams.

2. RESULTS AND DISCUSSION

2.1. Non-Isothermal Crystallization of PLA Blends. In thermal property aspects, there are two factors, i.e., melting behavior and crystallinity, that would affect the PLA's foaming behavior. Hence, these two thermal parameters were majorly studied. Figure 1 shows the differential scanning calorimetry (DSC) curves of a non-isothermal melting scan for PLLAs blended with DS and PPZn. From the DSC curves, PLA's crystallization temperature (T_c), cold crystallization temperature (T_{cc}), melting temperature (T_m), as well as crystallinity (X_c) were obtained, as shown in Table 1. It could be observed that PLLA/DS had clear double melting peaks in the DSC curves. However, PLLA/DS/PPZn only had one melting peak. The reason for the difference is the crystallization rate of PLA. Han et al. reported a similar phenomenon in PLA/PPZn nucleated blends. They found that the double melting peaks appeared with the addition of PPZn, but the thermal behavior gradually alleviated and disappeared with the increasing amount of PPZn.²¹ The formation mechanism of double melting peaks is closely related to the cold crystallization behavior of PLA. Some imperfect crystals formed through the cold crystallization mechanism in the quick heating process. Part of these imperfect crystals melted at lower temperatures.²² In crystallization aspects, the DSC results revealed that the crystallization-promoting effect of DS was weak as shown in Figure 1. The crystallinity of PLLA/DS was only 7.29%. Compared with that of DS, adding a small amount of PPZn could not suppress the cold crystallization of PLA. However, in the case of adding DS and PPZn simultaneously, its crystallinity increased to 33.12%, which was 19.83 times as high as that of pure PLLA. Interestingly, the crystallinity of PLLA/DS/PPZn decreased to 29.35% with the addition of CO_2 . It was anticipated that the addition of CO_2 could improve the chain mobility of PLA. However, the presence of CO_2 molecules in turn changed the interaction between PPZn, DS, and PLA chains. The CO_2 molecules were attracted to PPZn and DS due to the molecular polarity resulting in the inefficiency of crystallization-promoting agents, which led to a decrease of crystallinity of PLA from 33.12 to 29.35%. Besides, it was observed that the PLA's T_m value decreased from 155.7 to 150.3 $^{\circ}\text{C}$. This was due to the plasticizing effect of CO_2 and thus a lower processing temperature could be applied.²³

Figure 2 shows the DSC curves of non-isothermal melting scan for PLLA/PDLA blended with DS and PPZn. The related thermal properties are shown in Table 2. The addition of PPZn and DS could evidently affect the crystallization of Sc crystals. All the PLLA/PDLAs had an endothermic peak around 210–

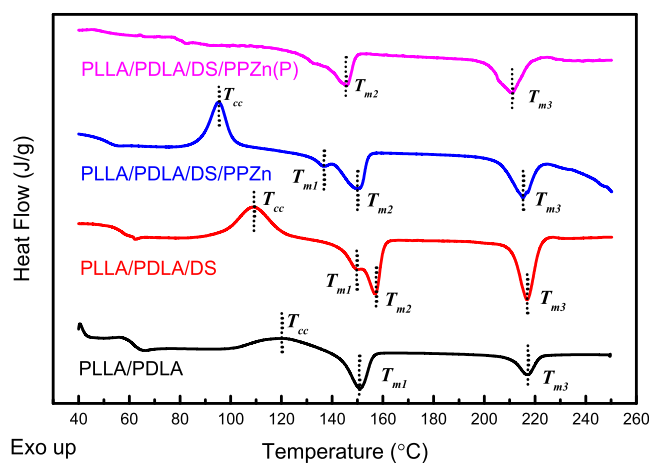


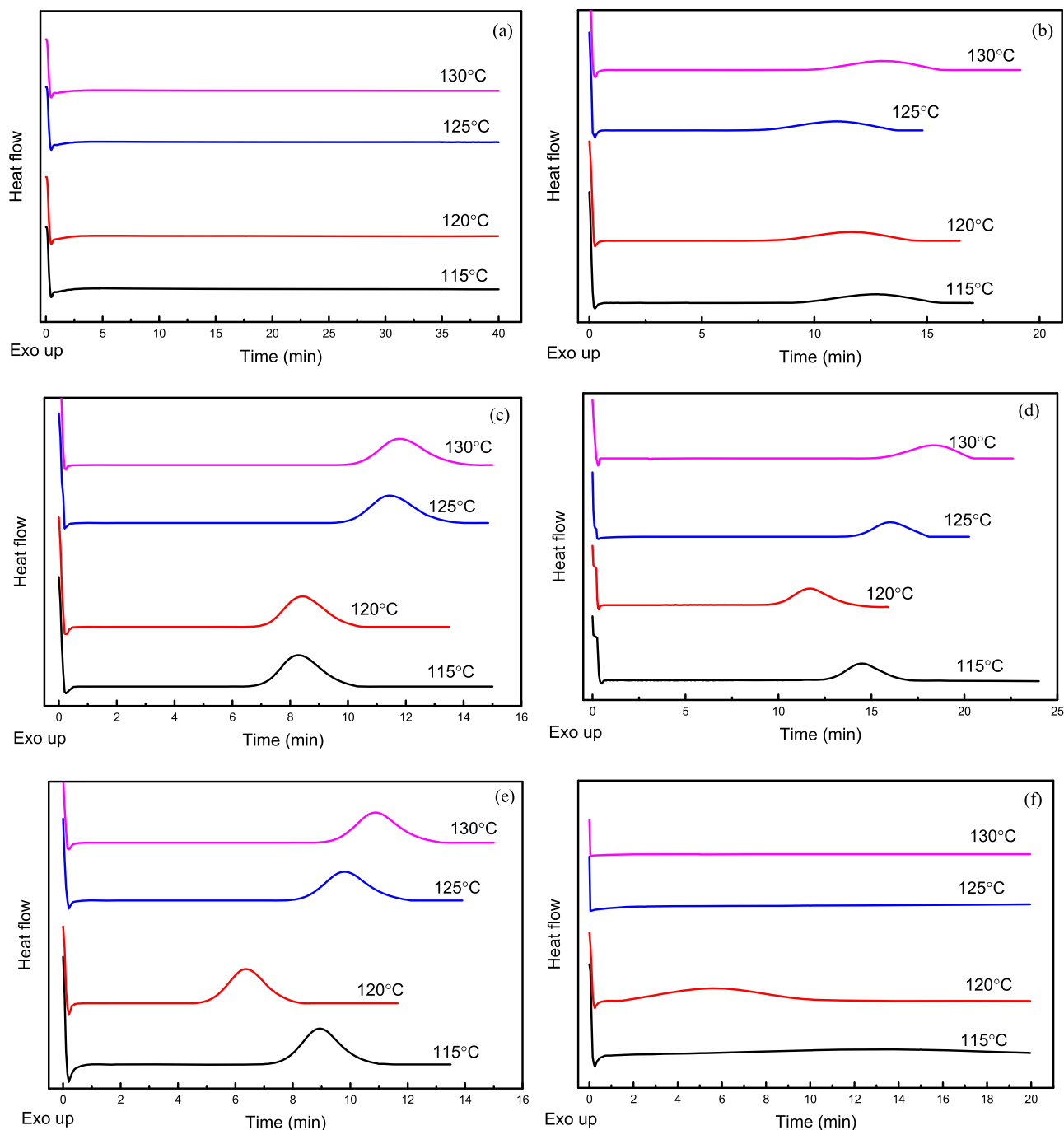
Figure 2. DSC curves of the PLLA/PDLA blends obtained with a heating rate of 10 $^{\circ}\text{C}/\text{min}$ under atmospheric and high-pressure conditions.

217 $^{\circ}\text{C}$, which was a typical melting peak of Sc crystals. It is worth noting that the addition of DS significantly changed the crystallization of Sc crystals in PLLA/PDLAs, thus increasing their crystallinity from 4.58 to 10.20%. However, in the case of PLLA/PDLA/DS/PPZn, the crystallinity of Sc crystals only slightly increased to 10.64%, which indicated that the simultaneous addition of DS and PPZn could promote the crystallization of α crystals rather than that of Sc crystals. This also indicated a stronger selective nucleation ability of PPZn. It should be noted that the theoretical maximum crystallinity of Sc crystals was 20% with the addition of 10 wt % PDLA because an equivalent mixture of enantiomeric PLLA and PDLA could form Sc crystals. Hence, we divided the Sc crystals by 20% to calculate each sample's absolute crystallinity (abs-crystallinity). The Sc abs-crystallinity of PLLA/PDLA/DS and PLLA/PDLA/DS/PPZn was about 50%. Pan et al. studied the effect of PPZn on the crystallization of PLLA/PDLA (50:50, w/w). They found that the Sc abs-crystallinity was 36.4%, which was obviously lower than that of PLLA/PDLA/DS.⁹ Therefore, the combined use of DS and PPZn had a strong effect on promoting Sc crystallization than the single use. As far as the crystallization-promoting effect of DS and PPZn was concerned, high-pressure CO_2 was induced into PLLA/PDLAs to increase the chain mobility of PLA. The crystallinity and abs-crystallinity of Sc were further increased to 12.44 and 62.20%, respectively. This implied that high-pressure CO_2 could promote the Sc crystallization even under non-isothermal conditions.

Moreover, the effect of the addition of DS and PPZn on the crystallization of α crystals in PLLA/PDLA was similar to that of PLLA. During the non-isothermal cooling process, the Sc crystals first formed from the molten PLA at a high temperature. The existing Sc crystals changed the crystallization of α crystals in the following cooling process. As shown in Table 2, the α crystallinities of PLLA/PDLAs were lower

Table 2. Thermal Property Parameters of the PLLA/PDLA Blends under Heating Conditions

sample	T_{cc}	Jcc/g	$T_m/^\circ\text{C}$	J_m/g	$X_c/\%$	$T_{sc}/^\circ\text{C}$	Jsc/g	$X_{sc}/\%$
PLLA/PDLA	120.0	17.05	150.6	19.86	3.00	217.4	6.50	4.58
PLLA/PDLA/DS	108.8	19.06	156.9	24.34	5.64	216.9	14.49	10.20
PLLA/PDLA/DS/PPZn	95.3	18.75	150.2	24.35	5.98	215.3	15.11	10.64
PLLA/PDLA/DS/PPZn(P)			145.5	19.08	20.38	210.7	17.67	12.44

**Figure 3.** DSC curves of (a) PLLA, (b) PLLA/PDLA, (c) PLLA/DS, (d) PLLA/PDLA/DS, (e) PLLA/DS/PPZn, and (f) PLLA/PDLA/DS/PPZn blends at various isothermal crystallization temperatures.

than those of PLLAs. For instance, PLLA/PDLA/DS/PPZn's crystallinity decreased from 33.12 to 5.98%. It exhibited a sharp cold crystallization peak in the DSC curve, while there was no obvious cold crystallization peak in the DSC curve of PLLA/DS/PPZn. Generally, it has commonly been assumed

that the existing Sc crystals could act as a crystallization nucleation agent to promote the heterogeneous nucleation of α crystals. The existing Sc crystals also affected the cold crystallization of PLA. Apparently, with the increase of the Sc crystallinity, the cold crystallization peak of PLA became

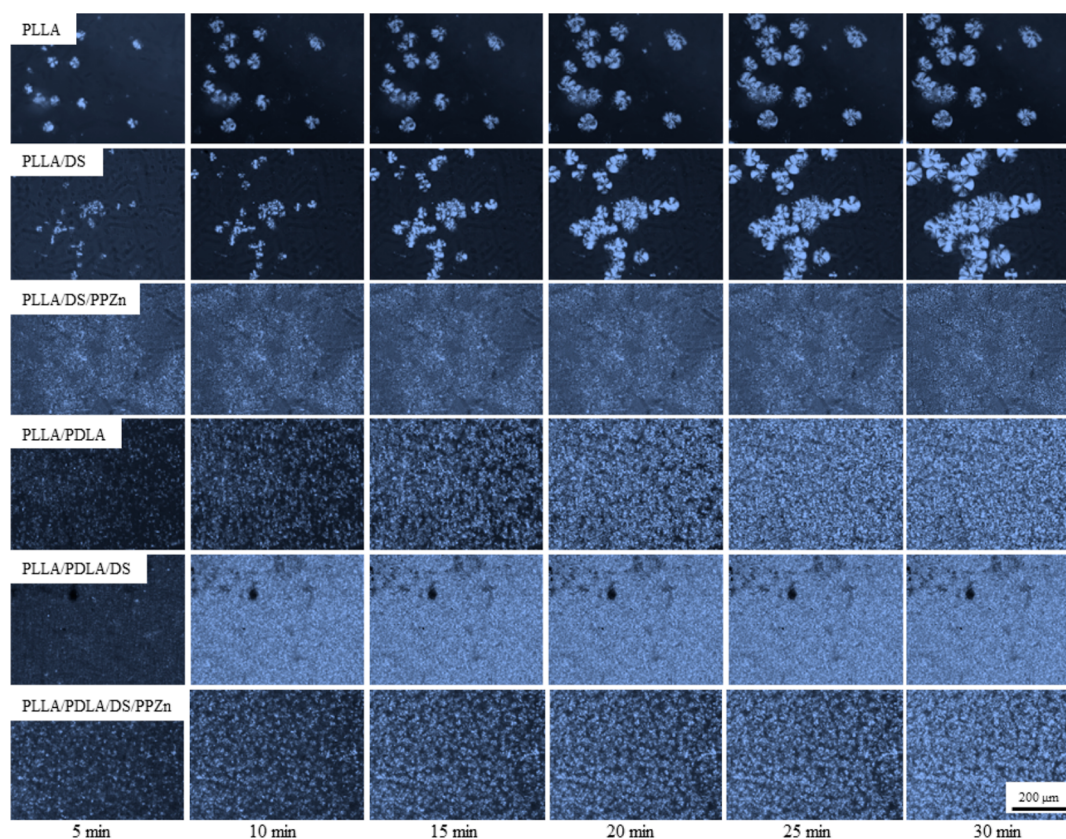


Figure 4. Crystal morphology of the PLA blends with isothermal crystallization at 120 °C for 30 min.

sharper and shifted to a lower temperature in the heating scanning. Li et al. also reported a similar phenomenon and its mechanism.²⁴ The existing Sc crystals acted as a crystallization nucleation agent to promote the formation of cold crystallization. Thus, cold crystallization could occur at relatively low temperatures in the heating. Thus, the α crystallinity increased from 1.67 to 3.00%, and T_{cc} decreased from 126.4 to 120 °C in the case of PLLA/PDLA. On the other hand, a competitive relationship existed between Sc crystallization and α crystallization. The higher the Sc crystallization, the more PLLA chains rearrange into the Sc crystal lattice. Thus, less PLLA chains can rearrange into the α crystal lattice, which results in a decrement of the α crystallinity. In order to further increase the Sc crystallinity, high-pressure CO₂ was used to assist the chain-rearranging ability, as shown in Figure 2. The Sc crystallinity of PLA increased from 10.64 to 12.44%, which was 2.72 times as high as that of PLLA/PDLA. However, more interestingly, the α crystallinity of PLA dramatically increased to 20.38%, which was 6.79 times as high as that of PLLA/PDLA. It demonstrated that the low α crystallinities of PLLA/PDLA/DS/PPZn were due to the poor mobility of PLA chains. Therefore, with the assistance of CO₂, PLA with both the high Sc crystallinity and high α crystallinity could be obtained in PLLA/PDLA. More importantly, PLA with various crystallinities and T_m were obtained, which could be used as modified materials for foaming purpose.

2.2. Isothermal Crystallization of PLA Blends. In order to study the effects of DS and PPZn on the crystallization rate of PLA, isothermal crystallization experiments at four different temperatures (115, 120, 125, and 130 °C) were carried out. Figure 3 shows the DSC curves of isothermal crystallization for

various PLA blends. We could observe the crystallization peak and its crystallization half-time from the curves. Due to the low crystallinity (<3%) and poor crystallization ability of PLLA, there was no obvious crystallization peak in the DSC curves at each isothermal temperature. However, the isothermal crystallization peaks appeared when adding 3 wt % DS into PLLA and PLLA/PDLA. The shortest half-times of the two samples occurred at an isothermal temperature of 120 °C, which were 8.4 and 11.7 min, respectively. In general, a high temperature condition (130 °C) favors the crystal growth, whereas a low temperature condition (115 °C) favors the crystal nucleation. An isothermal temperature of 120 °C is between the two temperatures, which is an ideal condition for rapid crystallization.²⁵ Hence, it was anticipated that the addition of DS could accelerate PLA's crystallization. The promoting effect of PLLA was stronger than that of PLLA/PDLA, which was consistent with the non-isothermal crystallization studies.

Based on this, the second component of PPZn was added to PLA/DS in order to further improve the crystallization rates. In the case of a crystallization temperature of 120 °C, the crystallization half-time of PLLA/DS/PPZn and PLLA/PDLA/DS/PPZn further decreased to 6.3 and 5.4 min, respectively. This change suggested that adding DS and PPZn simultaneously obviously facilitated the isothermal crystallization of PLA, thus increasing the crystallization rate. It was worth noting that the crystallization peak occurred only at 120 °C for PLLA/PDLA/DS/PPZn. The possible reason was that addition of DS and PPZn could improve only Sc crystallization (refer to Table 2). Thus, the number of PLA chains rearranged into the α crystal lattice decreased resulting in a low α crystallinity and an insignificant crystallization peak.

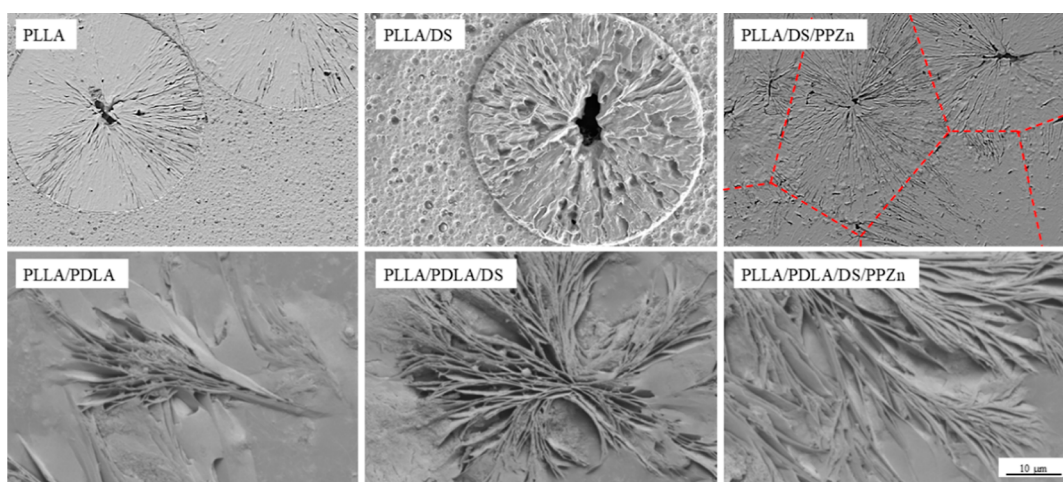


Figure 5. SEM images of non-isothermal crystals of the PLA blends etched by the solution of sodium hydroxide.

In conclusion, the added DS/PPZn served as not only an efficient crystallinity-promoting agent but also an excellent crystallization accelerator.

2.3. Crystallization Morphologies of PLA Blends. The crystalline structures of various PLA blends were observed by polarized optical microscopy (POM) at an isothermal temperature of 120 °C with a time interval of 5 min. As shown in Figure 4, the spherulite formation time of the six samples was 30, 30, 5, 15, 10, and 5 min, respectively. This spherulite growth trend was similar to the DSC results shown in Figure 3. Moreover, it is clear that pure PLLA crystallized in a typical homogeneous nucleation way. Its spherulite number was limited, and the spherulite size was around 100 μm. Besides, a typical characteristic birefringence pattern appeared in the POM photograph. Interestingly, there was no obvious isothermal crystallization peak at 120 °C as shown in Figure 3a. This contradiction was due to that DSC and POM characterized the PLA's crystallization behavior in different ways. In the case of low crystallinity of PLLA (1.67%), the crystallization peak in the isothermal DSC curve was too small to observe; but the small amount of spherulites could be observed using a polarized optical microscope. The introduction of DS to PLA increased the number of spherulites, while there was no change in the size of spherulites. As far as non-isothermal crystallization is concerned, it is believed that DS could affect the crystallinity rather than the nucleation mode. Upon further addition of PPZn to PLLA/DS, abundant small spherulites were generated, which can be observed in the POM photograph. The spherulite size sharply decreased to 12 μm, which means that PPZn could improve the crystallization nucleation of PLA. A similar phenomenon was observed in PLLA/PDLAs. However, the spherulite morphology of PLLA/PDLA was different from that of PLLAs. It was a typical central vertical slice of the banded spherulites.²⁶ While with the addition of DS, PLLA/PDLA shows a much higher crystallization nucleation density. The massive small spherulites filled up all the observation area. In addition, the spherulite size greatly decreased. This trend was very different from the crystals of PLLAs but was consistent with the previous DSC results. The unique spherulite morphology also implied that the addition of DS could efficiently improve the crystallinity of PLLA/PDLA (increased from 4.58 to 10.20%). Upon adding PPZn, more crystal zones formed. The greater number of nuclei and a small spherulite size suggested that the

nucleation of PLA crystals was easier with the simultaneous addition of DS and PPZn. Thus, PLA with a crystalline morphology of abundant and small spherulites could be obtained.

Figure 5 shows the microstructure features of the crystal morphology of PLLAs and PLLA/PDLAs. From the scanning electron microscopy (SEM) images, a few large and spherical skeletons could be found on the surface of PLLAs, while irregular flabellate skeletons with a radiating shape were found on the surface of PLLA/PDLAs. The two different crystalline structures belonged to α and Sc crystals according to the wide-angle X-ray diffraction (WAXD) results shown in Figure 6.

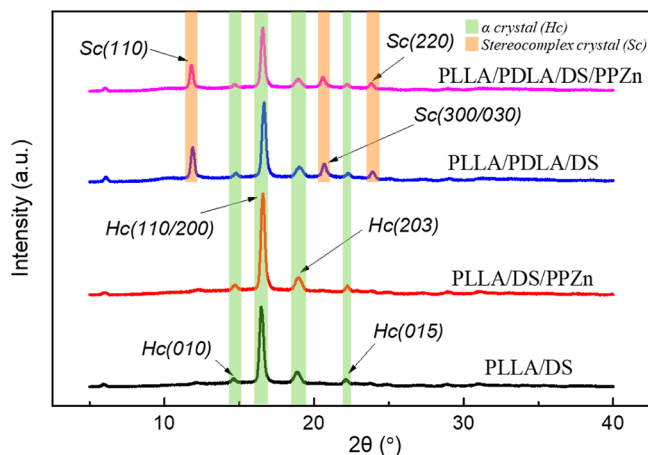


Figure 6. WAXD curves of non-isothermal crystals of the PLA blends.

PLLA/DS/PPZn exhibited a structure with numerous polygonal spherulites. This structure was due to the efficient heterogeneous nucleation effect of PPZn and sufficient isothermal crystallization time; thus, a large number of spherulites were in contact with each other during the crystal growth period, resulting in polygonal-shaped spherulites. The spherulite morphology proved the different crystallization nucleation ability resulting from adding DS and DS/PPZn.

Figure 6 shows the WAXD intensity curves of different PLA blends. The crystal diffraction peaks of all PLLA blends were located at 14.9° (010), 16.7° (110/200), 19.1° (203), and 22.3° (015). These peaks were all characterized to be α crystals of PLA,²⁷ indicating that the crystal form of PLA was not

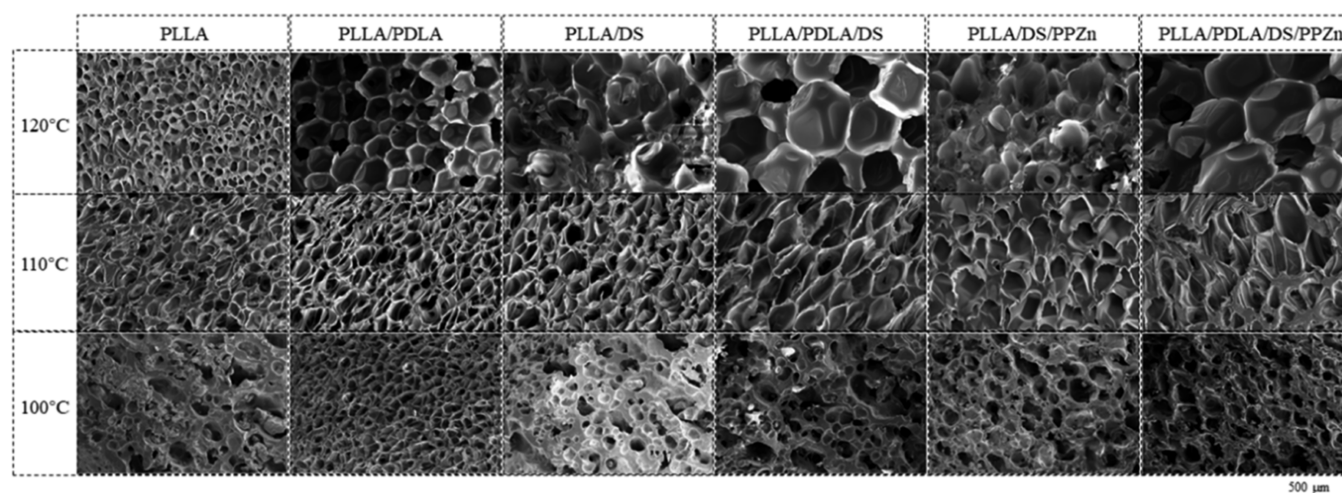


Figure 7. SEM images of the foamed PLA blends at different foaming temperatures.

Table 3. Cellular Structure Parameters of the Foamed PLA Blends

foaming temperature (°C)	samples	crystallinity (%)	density (g/cm ³)	expansion ratio	cell density (cell/cm ³)	cell size (μm)
120	PLLA	1.67	0.189	6.6	4.17×10^6	104 + 63–31
	PLLA/PDLA	6.08	0.118	10.6	9.21×10^5	241 + 11–38
	PLLA/DS	0	0.128	9.8	4.31×10^5	275 + 220–93
	PLLA/PDLA/DS	10.20	0.083	15.0	3.11×10^5	411 + 201–99
	PLLA/DS/PPZn	0	0.158	7.9	5.53×10^5	255 + 116–102
	PLLA/PDLA/DS/PPZn	10.64	0.077	16.2	3.61×10^5	545 + 107–203
110	PLLA	1.67	0.231	5.4	2.07×10^6	132 + 41–42
	PLLA/PDLA	7.58	0.169	7.4	4.39×10^6	211 + 30–28
	PLLA/DS	7.29	0.198	6.3	2.63×10^6	129 + 34–25
	PLLA/PDLA/DS	10.20	0.134	9.3	7.17×10^5	254 + 57–62
	PLLA/DS/PPZn	0	0.231	5.4	4.97×10^5	178 + 98–75
	PLLA/PDLA/DS/PPZn	10.64	0.147	8.5	8.26×10^5	223 + 140–113
100	PLLA	1.67	0.595	2.1	2.73×10^5	127 + 184–75
	PLLA/PDLA	7.58	0.245	5.1	3.70×10^6	139 + 43–66
	PLLA/DS	7.29	0.391	3.2	6.76×10^5	135 + 61–64
	PLLA/PDLA/DS	15.80	0.321	3.9	6.84×10^5	123 + 101–71
	PLLA/DS/PPZn	0	0.338	3.7	5.35×10^5	147 + 115–101
	PLLA/PDLA/DS/PPZn	10.64	0.291	4.3	8.23×10^5	159 + 72–117

changed by the strategy of adding DS and PPZn. For the PLLA/PDLA blends, besides the diffraction peaks of α crystals, extra characteristic diffractions peaks occurred at 12.0, 20.8, and 24.0°, which correspond to the (110), (300/030), and (220) crystalline planes of Sc crystals, respectively.²⁸ This indicated the coexistence of α crystals and Sc crystals. However, the characteristic diffractions of Sc crystallites were stronger in PLLA/PDLAs; while those of α crystallites were relatively weaker compared with that of PLLAs. It suggests the competitive relationship between the α crystallization and the Sc crystallization. The generation of Sc crystals could restrict the formation of α crystals, which was in agreement with the DSC results.

2.4. Foaming Behavior of PLA Blends. Figure 7 and Table 3 display the cellular morphologies of the PLA blends at three different foaming temperatures and the corresponding cellular parameters. The cellular structures of PLA foams could be changed via different crystallization-induced methods.

The foaming temperature is a factor that controls the cellular structure of the PLA foam. As shown in Figure 7, all the PLA foams exhibited a separated-sphere cellular morphology with a non-uniform cell size at a low foaming temperature (100 °C).

The main reason was that the high melt viscosity of PLA arising from the low temperature brought extra resistance to cell growth; thus, the cells in the PLA matrix were difficult to grow to a large size and finally remained in a spherical morphology. In the case of the medium foaming temperature condition (110 °C), the resistance to cell growth reduced with the decrease of melt viscosity. Based on that, cells in the PLA matrix could further grow to contact and impact each other, which led to a polyhedral cellular morphology. The cellular parameters as shown in Table 3 implied that both the cell size and expansion ratio increased with the increment of foaming temperature. The greatest change in the cellular structure occurred in PLLA/PDLA/DS. Its expansion ratio and cell size increased from 3.9 and 123 to 9.3 and 254 μm, respectively. A further increase of the foaming temperature to 120 °C brought a very low melt viscosity and weak cell growth resistance. At this foaming temperature, most of the PLA foams exhibited a typical polyhedral cellular morphology. However, PLLA/DS and PLLA/DS/PPZn foams exhibited an open-cell structure with many cells ruptured, which resulted from the crystallization property. The addition of DS increased only the crystallinity of PLA but did not improve the spherulite

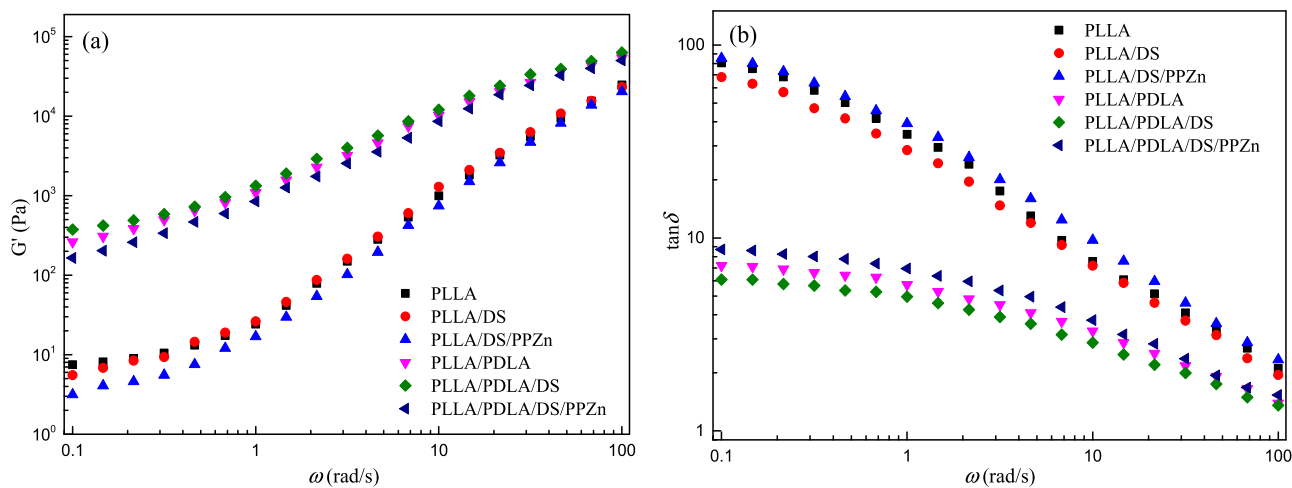


Figure 8. (a) Storage modulus curves and (b) loss factor curves of the PLLA blends and the PLLA/PDLA blends.

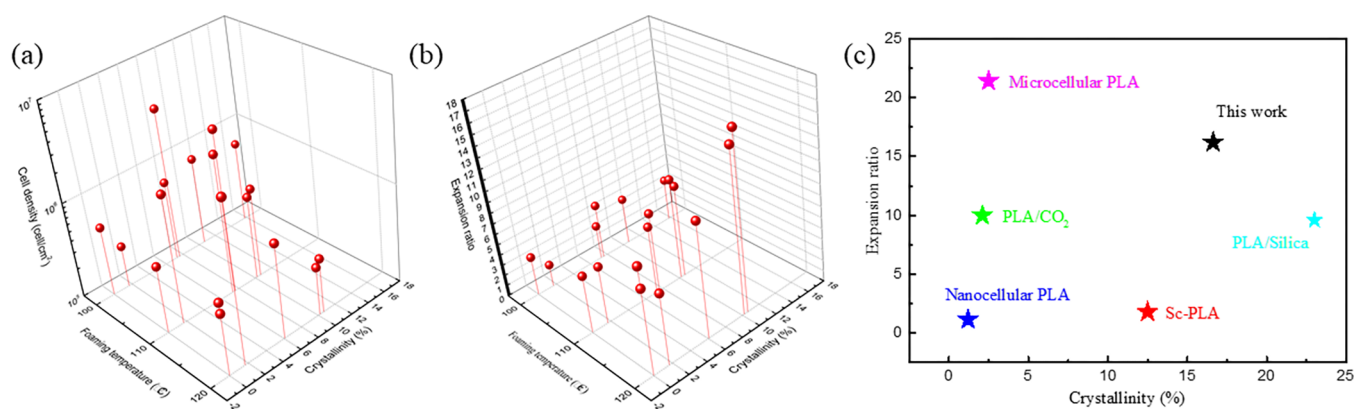


Figure 9. (a) Relationships between crystallinities and cell density of the PLA blends at different foaming temperatures. (b) Relationships between crystallinities and the expansion ratio of the PLA blends at different foaming temperatures. (c) Ashby plots of crystallinity before foaming and the expansion ratio of the reported PLAs without chemical modification, including Sc-PLA,³² PLA/CO₂,³³ nanocellular PLA,³⁴ PLA/silica,³⁵ and microcellular PLA.³⁶

morphology (refer to Figure 4). Table 3 also shows that the foaming temperature had a more significant effect on the cellular structure of PLLA/PDLA/DS/PPZn. Its expansion ratio and cell size increased from 4.3 and 159 to 16.2 and 545 μm , respectively. Hence, it was anticipated that the change in the foaming temperature would control the melt viscosity of PLA in the foaming process. The higher the foaming temperature, the lower the melt viscosity was, thus the larger the cell size was.

In order to study the effect of Sc crystals on the foamability of PLA, dynamic shear rheological experiments were carried out. Figure 8a shows the relationship of the storage modulus (G') of the PLLA blends and the PLLA/PDLA blends versus the angle frequency. The change of melt elasticity could be directly characterized by the increase of the G' value. It could be observed that the G' values of the PLLA/PDLA blends were much higher than those of PLLA blends. This was due to the chain physical entanglements caused by the Sc crystals in the matrix. Figure 8b shows the relationship of loss angle ($\tan \delta$) of the PLLA blends and the PLLA/PDLA blends as a function of angular frequency. The lag angle, δ , is the angle that the stress lagged behind the strain while the melt was under an alternating stress field. The term $\tan \delta$ refers to the ratio of viscous to elastic contributions. The smaller the $\tan \delta$, the faster the melt elastic response was and the greater the melt

elasticity was. In the case of PLLA/PDLA blends, the $\tan \delta$ values were related to the chain entanglement structure. The $\tan \delta$ values of PLLA blends were higher, which is a typical terminal behavior of liquid-like melts. The $\tan \delta$ values of the PLLA/PDLA blends were obviously smaller than those of PLLA blends at the same frequency, which implied that the elastic contribution was increased by the existence of Sc crystals. The Sc crystals acted as physical network points; therefore, the melt strength of PLA was improved, which was favorable for the foaming purpose.

The crystallinity of PLA at a constant foaming temperature is the second factor that affects the cellular structure of the PLA foam. As shown in the previous DSC results, different PLAs had different T_m values and crystallinities. Therefore, PLAs may be in the melt state, crystalline state, or melt/crystalline transition state at a certain foaming temperature. Figure 9 shows the relationships between the crystallinities and the cellular structure parameters of various PLA blends at different foaming temperatures. The mentioned crystallinity value is the sum value of α crystallinity and Sc crystallinity. The crystallinity value equals half of the crystallinity of the crystal form when the foaming temperature is close to the melting peak temperature. As shown in Figure 9a, PLA with proper crystallinity ($\sim 6\%$) had the highest cell density of 10^6 cell/cm³, whereas the cell density was only 10^5 cell/cm³ for either high

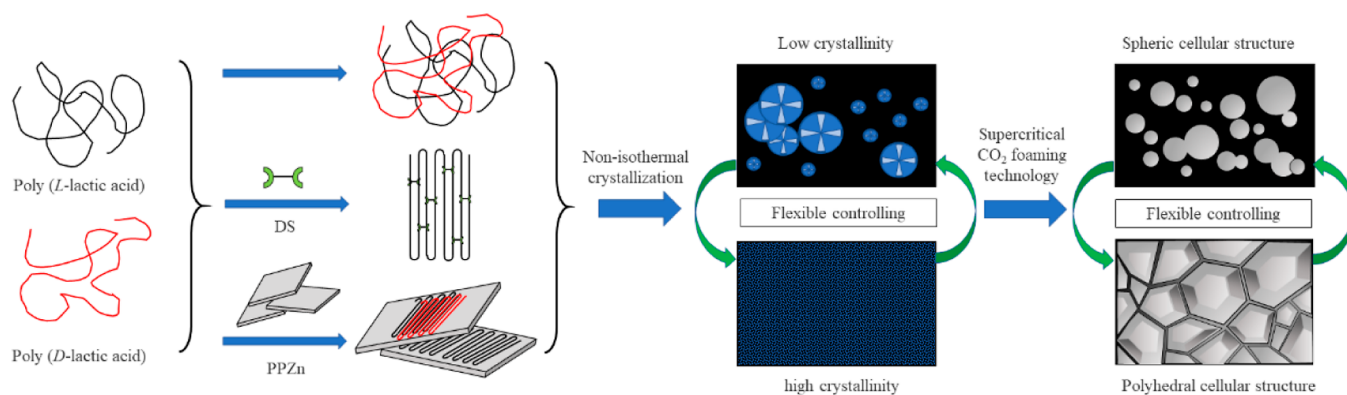


Figure 10. Schematic of the mechanism for controlling the cellular structures of the PLA blends.

or low crystallinity. This could be attributed to the heterogeneous nucleation capability of the crystalline zones. When crystallinity was low, the heterogeneous nucleation effect was weak, resulting in a low cell density. When crystallinity was 10% or above, the volume fraction of foamable amorphous PLA reduced and the cell growth resistance increased, also resulting in a low cell density. Figure 9b shows the relationship of the expansion ratio, the foaming temperature, and the crystallinity. With the increase of the foaming temperature from 100 to 120 °C, the expansion ratio of PLA foams was obviously increased due to the decrease of the melt viscosity. The cells were easier to grow bigger because the cell growth resistance was reduced. It also demonstrated that achieving proper crystallinity could be adopted as an effective method to form a fine cell structure and a high expansion ratio foam. This is because a proper crystallinity reduced the escape of foaming gases.^{29,30} Interestingly, in the case of PLLA/PDLA/DS/PPZn, it had the highest crystallinity of 32.82%; however, its foam also had the highest expansion ratio of 16.2. The reason was that its high crystallinity was mainly due to the Sc crystals. In the previous study, we revealed that the presence of Sc crystals could facilitate the improvement of PLA's foamability.³¹ Therefore, controlling the crystallinity could change the foaming structure parameters.

The addition of various crystallization-promoting agents is the third factor that controls the cellular structure of the PLA foam. The DSC results indicated that the addition of PDLA, DS, and PPZn could change the PLA's crystal form and crystallinity. The crystallinity of PLA blends varied from 0 to 17% in the foaming process. For the purpose of improving the expansion ratio, the synergistic effect of DS with PPZn was generally stronger than the effect of using DS solely. However, for the purpose of enhancing the cell density, adding DS alone was effective than adding DS and PPZn simultaneously.

Therefore, adding various crystallization-promoting agents led to different crystals, T_m values, and crystallinities of PLA. This, in turn, had a dramatic effect on foamability, which led to different cellular morphologies of PLA. Thus, a variety of PLA foams with various cellular morphologies could be obtained through the crystallization-induced strategy. The PLLA/PDLA/DS/PPZn shows high crystallinity (16.22%) and expansion ratio value (16.2), which surpass those of most of the PLA foams without chemical modification published previously as shown in Figure 9c.

2.5. Mechanisms. Figure 10 shows the schematic of the mechanism of crystallization-induced foaming technology of

PLA. Mixing PLLA with PDLA could induce the unmolten Sc crystals in the foaming process. However, adding DS and PPZn could further control the crystallinity and fraction of Sc crystals and α crystals. The predominant mechanisms of improving PLA crystallization through adding DS and PPZn were different. The melting point of DS was around 93 °C. At 190 °C, DS and PLA were both in molten states. Hence, DS easily disperses at the molecular level in the PLA matrix. On cooling, the hydrogen bonding interaction between the hydroxyl groups of DS and the carbonyl groups of PLA chains could be effectively developed. This hydrogen bonding twisted and folded the PLA chain segments to promote the orderly stacking of PLA chains, which favored the crystallization nucleation.³⁷ The detailed mechanism is shown in Supporting Information, Figure S3. Moreover, in PPZn's chemical structure, the metal ions, Zn^{2+} , could form an inner polar layer shielded by two non-polar layers of aromatic rings. These non-polar surfaces interacted through weak van der Waals contacts, which were easily exfoliated. In crystallization, the PLA crystals would epitaxially grow on the surface of exfoliated PPZn. The growth of one crystal on the other was controlled by matching the two lattice planes in contact. PPZn possessed an orthorhombic cell with lattice parameters $a = 0.566$ nm, $b = 1.445$ nm, and $c = 0.480$ nm. In PLA α crystals, the chains were packed in an orthorhombic unit cell with dimensions $a = 1.034$ nm, $b = 0.597$ nm, and $c = 2.88$ nm. The length of the c axis of α crystals was twice that of the b axis of PPZn, with a tiny mismatching value of 0.3%. This excellent matching suggested that PLA crystals could grow on the PPZn surface via a template mechanism.³⁸ The detailed mechanism is shown in Supporting Information, Figure S4. By means of the above adding strategies, PLA with a highly controllable crystalline morphology, high crystallinity, as well as rapid crystallization could be obtained even in a non-isothermal cooling process (refer to Figures 1 and 2 and Tables 1 and 2). The induced crystallization affected the foaming behavior in two aspects. First, the dissolution and transport of CO₂ molecules in the PLA matrix only occurred in the amorphous phase, while the crystalline phase acted as a barrier for diffusing CO₂ molecules. Thus, the crystallinity also provided a resistance to cell growth, disrupting the aggressive foaming trends and ensuring a fine cell structure.³⁹ Second, the cell nucleation was controlled by the crystallization of PLA. The activation energy barrier of cell nucleation on the spherulite surfaces was low, which means that more cells could form around the spherulites via a heterogeneous nucleation mechanism.⁴⁰ Hence, cells in the PLA matrix could nucleate and grow more efficiently in the

foaming process. This led to a foam with a high cell density. The presence of Sc crystals could improve PLA's foamability, which in turn increase the expansion ratio of the PLA foam. Consequently, inducing desirable crystallization property of PLA could facilitate the foaming process to change the cell nucleation and growth paths. Thus, a PLA foam with a high expansion ratio and a uniform cellular morphology can be easily prepared.

3. CONCLUSIONS

As described above, a novel crystallization-promoting agent (DS/PPZn/CO₂) was developed to improve PLA's crystallization and to control its foaming behavior. In the process, DS and PPZn could serve as efficient crystallization modifiers for changing the crystallinity and T_m of PLA. The results showed that adding DS and PPZn simultaneously could increase the α crystallinity of PLA from 1.67 to 33.12%, which was 19.38 times that of PLLA. As for Sc crystals, adding DS could increase the Sc crystallinity of PLA from 4.58 to 10.20%, but adding DS and PPZn simultaneously could only increase the Sc crystallinity of PLA to 10.64%. It also demonstrated that PPZn had a stronger selective nucleation ability for α /Sc crystal forms. Moreover, with the assistance of a high-pressure CO₂ fluid, the Sc crystallinity of PLA could further increase to 12.44%. In brief, PLA with a high α crystallinity was prepared by adding DS and PPZn, and PLA with a high Sc crystallinity could be prepared by adding DS. Subsequently, a variety of cellular morphologies were developed by changing crystallization behaviors. The foaming experiments revealed that PLA with a fine spherulite morphology, a crystallinity of 6%, and rapid crystallization ability had the highest cell density of 4.36×10^6 cell/cm³. Besides, when the foaming temperature was higher than the T_m of α crystals, and the Sc crystallinity was above 10%, PLA had a superior melting strength and its foaming expansion ratio could reach 16.2. A variety of cellular morphologies of PLA foams could be obtained by changing the foaming temperature and the crystallization property. In a word, controlling the Sc/ α crystallinity and T_m of α crystals is an efficient approach for optimizing the foamability of PLA.

4. EXPERIMENTAL SECTION

4.1. Materials. PLLA (2002D) with a 96 mol % L-isomeric content and a molecular weight of 15,000 g/mol was purchased from NatureWorks, USA. PDLA (13000 C) with a 99 mol % D-isomeric content and a molecular weight of 13,000 g/mol was obtained from Dai Gang, China. DS (analytical reagent) was supplied by Aladdin, China. PPZn was synthesized according to a previously reported procedure.⁴¹

4.2. Preparation of PLA Blends and Their Foams.

4.2.1. Synthesis of PPZn. First, phenylphosphonic acid was dissolved in water to form a solution with a concentration of 0.025 g/mL. One equivalent of ZnCl₂ was also dissolved in water and then added to the stirred phenylphosphonic acid solution, followed by the addition of 0.1 mol/L aqueous HCl to reach a pH of 5–6. After that, the solution was filtered and stirred in water at 50 °C for 36 h to improve the crystallinity. The resultant product was filtered, washed with water, and dried at 40 °C for 24 h. Finally, the resultant PPZn was obtained through dehydration at 150 °C for 8 h.

4.2.2. Preparation of PLA Blends. The ingredients were dried at 60 °C for 4 h to remove excess surface moisture. After that, the resins, PLLA and PDLA, were mixed with DS and

PPZn using a torque rheometer (XSS60, Kechuang, China) with a rotor speed of 60 rpm at 190 °C for 8 min. As a control sample, pure PLLA or PLLA/PDLA was mixed under the same conditions. The resultant blends were cut into small pellets and were pressed by compression-molding into a sheet form (2 mm × 10 mm × 10 mm) at 190 °C for 10 min. Then, the PLA blend sheets were cooled down to 20 °C at a cooling rate of 10 °C/min using a compressor (LP-S-50, Labtech, Thailand). After that, the samples were taken out for the subsequent characterizations and foaming process (the photographs of PLA blends are shown in Supporting Information, Figure S1). All ingredients used in the formula are presented in Table 4.

Table 4. Weight Ratio of Each Component of the PLA Blends (Unit: wt %)

serial no.	PLLA	PDLA	DS	PPZn
PLLA	100	0	0	0
PLLA/PDLA	90	10	0	0
PLLA/DS	97	0	3	0
PLLA/DS/PPZn	94	0	3	3
PLLA/PDLA/DS	87.3	9.7	3	0
PLLA/PDLA/DS/PPZn	84.6	9.4	3	3

4.2.3. Preparation of PLA Foams. The PLA foams were prepared by the solid-state foaming technology using supercritical CO₂ as a blowing agent (the details of the foaming apparatus are shown in Supporting Information, Figure S2). First, the PLA blends were placed in a customized autoclave. Then, the samples in the autoclave were heated to the foaming temperature at a rate of 10 °C/min using a programmed temperature controller. The foaming temperature for each sample was set to 100, 110, and 120 °C, respectively. The foaming pressure and saturation time were set to 20 MPa and 5 h, respectively. The injection of the supercritical CO₂ fluid was achieved by using a syringe pump. A pressure transducer was used to measure the pressure and a needle valve to release pressure. When CO₂ completely diffused and dissolved into PLA, a sudden pressure drop by the release of CO₂ from 20 to 0.1 MPa provided the driving force for cell growth. After that, the foamed samples were cooled down to 30 °C at a cooling rate of 20 °C/min in the autoclave, and were taken out from the autoclave for the subsequent characterizations.

4.3. Analysis. **4.3.1. Non-Isothermal Crystallization Analysis.** The non-isothermal crystallization behaviors of the PLA blends were characterized using a high-pressure differential scanning calorimetry (HP-DSC) system (HP204, Netzsch, Germany) purged with nitrogen. All the PLA blends were tested under two different pressure conditions (atmospheric pressure and 5 MPa CO₂ pressure). The PLLA blends were heated to 200 °C at a rate of 10 °C/min to study the effects of DS and PPZn on the non-isothermal crystallization of α crystals, while the PLLA/PDLA blends were heated to 250 °C at a rate of 10 °C/min to study the non-isothermal crystallization of Sc/ α crystals induced by the addition of PPZn and DS.

The α and Sc crystallinity of PLA, χ_c and χ_{Sc} , were calculated using eqs 1 and 2, respectively

$$\chi_c = \frac{\Delta H_m - \Delta H_{cc}}{\Delta H_c^0 \times (1 - w_f)} \times 100\% \quad (1)$$

42

$$\chi_{sc} = \frac{\Delta H_m}{\Delta H_c^0 \times (1 - w_f)} \times 100\% \quad (2)$$

⁴³ where ΔH_m and ΔH_c are the melting enthalpy and the cold crystallization enthalpy, respectively. w_f is the weight fraction of the crystallization-promoting agent in the blends. The α and Sc melting enthalpies of 100% crystalline PLA are 93.6 and 142 J/g, respectively.⁴⁴

4.3.2. Isothermal Crystallization Analysis. The isothermal crystallization behaviors of the PLA blends were also studied by HP-DSC. All the samples were first eliminated thermal histories. Then, the samples were cooled down at a rate of 40 °C/min to the isothermal temperatures of 115, 120, 125, and 130 °C. The effects of DS and PPZn on the isothermal crystallization of PLA samples were studied.

4.3.3. Crystalline Form Analysis. The crystalline form of PLA blends was measured by WAXD (SmartLab, Rigaku, Japan). The X-ray source was Cu Ka radiation ($\lambda = 1.542 \text{ \AA}$). The diffractometer was operated at 30 kV and 15 mA, from 5 to 40° at a scan rate of 2°/min.

4.3.4. Crystalline Morphology Observation. The morphology of the crystalline zone was observed using a scanning electron microscope (Nova-Nano450, FEI, USA). In order to investigate the spherulite's surface morphology, PLA blends were heat compressed into a film form with 300 μm thickness on a heating stage at 200 °C and then cooled to room temperature at a cooling rate of 10 °C/min. After that, the film samples were etched at 25 °C in a solution of 0.025 mol/L NaOH in water–methanol (1:2, v/v) for 7 h. Then, the etched samples were dried in a vacuum oven at 50 °C. Before SEM observation, the samples were coated with gold using a sputter coater (K550X, Quorum Technologies, Britain).

The spherulite morphologies of PLA blends were observed using a polarized optical microscope (BX-51, Olympus, Japan) equipped with a CCD camera. The samples were heated from room temperature to 200 °C at 20 °C/min, held there for 5 min, then cooled to 120 °C at a cooling rate of 20 °C/min and held for 20 min. The magnification ratio was 500.

4.3.5. Foaming Property Characterizations. The densities of unfoamed and foamed samples, ρ and ρ_f , were measured using a density balance (BSA623S, Sartorius, Germany). The expansion ratio of the PLA foam is equal to ρ divided by ρ_f .

The cellular structures of PLA foams were observed using a scanning electron microscope at an acceleration voltage of 3 kV. The magnification ratio was 400. The mean cell density, N_c , can be calculated according to eq 3

$$N_c = \left(\frac{N}{A}\right)^{3/2} \times \text{expansion ratio} \quad (3)$$

⁴⁵ where N and A are the number of cells observed in the SEM image and the area of the SEM image, respectively. The mean cell size value, R , can be calculated using eq 4

$$R = \left(\frac{\sum_{i=1}^{N_0} r_i^3}{N}\right)^{1/3} \quad (4)$$

⁴⁶ where r_i is the cell size of each cell measured by Image-Pro Plus software.

4.3.6. Rheological Analysis. Rheological parameters of PLA blends were recorded using a strain-controlled rheometer (MARS Rheometer, Thermo Fisher, USA). The testing temperature and fixture were 190 °C and parallel plates with

a diameter of 20 mm and a gap of 1.0 mm, respectively. The testing frequency range was set to 0.1–100 rad/s. The maximum strain was fixed at 5% to confirm the linear viscoelastic region. The storage modulus and loss factor values were recorded at different frequencies.

■ ASSOCIATED CONTENT

Supporting Information

The Supporting Information is available free of charge at <https://pubs.acs.org/doi/10.1021/acsomega.1c06777>.

Photographs of PLA blends; schematic diagram of a supercritical CO₂ solid-state foaming apparatus; schematic diagram of crystallization promotion by D-sorbitol; and schematic diagram of crystallization promotion by PPZn (PDF)

■ AUTHOR INFORMATION

Corresponding Author

Chun Zhang – School of Materials and Energy Engineering, Guizhou Institute of Technology, Guiyang 550003, China; orcid.org/0000-0003-3038-6269; Email: zhangchun925@126.com

Authors

Wei Liu – School of Materials and Energy Engineering, Guizhou Institute of Technology, Guiyang 550003, China; orcid.org/0000-0002-9908-1829

Xian Wu – School of Materials and Energy Engineering, Guizhou Institute of Technology, Guiyang 550003, China

Xiao Cheng Chen – School of Materials and Energy Engineering, Guizhou Institute of Technology, Guiyang 550003, China

Shan Liu – School of Materials and Energy Engineering, Guizhou Institute of Technology, Guiyang 550003, China

Complete contact information is available at:

<https://pubs.acs.org/doi/10.1021/acsomega.1c06777>

Notes

The authors declare no competing financial interest.

■ ACKNOWLEDGMENTS

We acknowledge the support from the National Natural Science Foundation of China (52163011, 51863003), the research Program of Talented Scholars of Guizhou Institute of Technology (XJGC20190657), and the Academic Novice Cultivation and Innovation Exploration Project (GZLGM-22) of Guizhou Provincial Science and Technology Department. We are thankful for some experimental works of Weiya Zhu and Xiaoqiong Cheng.

■ REFERENCES

- Ni, J.; Yu, K.; Zhou, H.; Mi, J.; Chen, S.; Wang, X. Morphological evolution of PLA foam from microcellular to nanocellular induced by cold crystallization assisted by supercritical CO₂. *J. Supercrit. Fluids* **2020**, *158*, 104719–104729.
- Chen, Y.; Weng, C.; Wang, Z.; Maertens, T.; Fan, P.; Chen, F.; Zhong, M.; Tan, J.; Yang, J. Preparation of polymeric foams with bimodal cell size: An application of heterogeneous nucleation effect of nanofillers. *J. Supercrit. Fluids* **2019**, *147*, 107–115.
- Lv, Z.; Zhao, N.; Wu, Z.; Zhu, C.; Li, Q. Fabrication of Novel Open-Cell Foams of Poly(ϵ -caprolactone)/Poly(lactic acid) Blends for Tissue-Engineering Scaffolds. *Ind. Eng. Chem. Res.* **2018**, *57*, 12951–12958.

- (4) Kuang, T.-R.; Mi, H.-Y.; Fu, D.-J.; Jing, X.; Chen, B.-y.; Mou, W.-J.; Peng, X.-F. Fabrication of Poly(lactic acid)/Graphene Oxide Foams with Highly Oriented and Elongated Cell Structure via Unidirectional Foaming Using Supercritical Carbon Dioxide. *Ind. Eng. Chem. Res.* **2015**, *54*, 758–768.
- (5) Liu, W.; Wu, X.; Ou, Y.; Liu, H.; Zhang, C. Electrically conductive and light-weight branched polylactic acid-based carbon nanotube foams. *E-Polymers* **2021**, *21*, 96–107.
- (6) Li, B.; Zhao, G.; Wang, G.; Zhang, L.; Gong, J.; Shi, Z. Biodegradable PLA/PBS open-cell foam fabricated by supercritical CO₂ foaming for selective oil-adsorption. *Sep. Purif. Technol.* **2021**, *257*, 117949–117959.
- (7) Wang, W.; Zhang, B.; Li, M.; Li, J.; Zhang, C.; Han, Y.; Wang, L.; Wang, K.; Zhou, C.; Liu, L.; Fan, Y.; Zhang, X. 3D printing of PLA/n-HA composite scaffolds with customized mechanical properties and biological functions for bone tissue engineering. *Composites, Part B* **2021**, *224*, 109192–110202.
- (8) Najafi, N.; Heuzey, M.-C.; Carreau, P. J.; Therriault, D.; Park, C. B. Rheological and foaming behavior of linear and branched polylactides. *Rheol. Acta* **2014**, *53*, 779–790.
- (9) Meng, X.; Shi, G.; Wu, C.; Chen, W.; Xin, Z.; Shi, Y.; Sheng, Y. Chain extension and oxidation stabilization of Triphenyl Phosphite (TPP) in PLA. *Polym. Degrad. Stab.* **2016**, *124*, 112–118.
- (10) Samuel, C.; Barrau, S.; Lefebvre, J.-M.; Raquez, J.-M.; Dubois, P. Designing multiple-shape memory polymers with miscible polymer blends: evidence and origins of a triple-shape memory effect for miscible PLLA/PMMA blends. *Macromolecules* **2014**, *47*, 6791–6803.
- (11) Kong, W.-L.; Bao, J.-B.; Wang, J.; Hu, G.-H.; Xu, Y.; Zhao, L. Preparation of open-cell polymer foams by CO₂ assisted foaming of polymer blends. *Polymer* **2016**, *90*, 331–341.
- (12) Riou, M.; Ausias, G.; Grohens, Y.; Gaudry, T.; Veillé, J.-M.; Férec, J. Thermoplastic foaming with thermo-expandable micro-capsules: Mathematical modeling and numerical simulation for extrusion process. *Chem. Eng. Sci.* **2020**, *227*, 115852–115862.
- (13) Li, Y.; Yin, D.; Liu, W.; Zhou, H.; Zhang, Y.; Wang, X. Fabrication of biodegradable poly (lactic acid)/carbon nanotube nanocomposite foams: significant improvement on rheological property and foamability. *Int. J. Biol. Macromol.* **2020**, *163*, 1175–1186.
- (14) Niu, D.; Xu, P.; Sun, Z.; Yang, W.; Dong, W.; Ji, Y.; Liu, T.; Du, M.; Lemstra, P. J.; Ma, P. Superior toughened bio-compostable Poly(glycolic acid)-based blends with enhanced melt strength via selective interfacial localization of in-situ grafted copolymers. *Polymer* **2021**, *235*, 124269–124279.
- (15) Foglia, F.; De Meo, A.; Iozzino, V.; Volpe, V.; Pantani, R. Isothermal crystallization of PLA : Nucleation density and growth rates of α and α' phases. *Can. J. Chem. Eng.* **2020**, *98*, 1998–2007.
- (16) Martín-de León, J.; Bernardo, V.; Solórzano, E.; Rodríguez-Pérez, M. A. New non-destructive optical approach to determine the crystallization kinetics of PLA under a CO₂ atmosphere with spatial and temporal resolution. *Polym. Test.* **2021**, *98*, 107201–107211.
- (17) Liu, G.; Yang, F.; Liu, W.; Jiao, W.; He, X.; Wang, R. Crystalline polymer functionalized non-oxidized graphene flakes for high gas barrier composites. *Int. J. Hydrogen Energy* **2021**, *46*, 5472–5484.
- (18) Črešnar, K. P.; Zemlji, L. F.; Papadopoulos, L.; Terzopoulou, Z.; Pissis, P. Effects of Ag, ZnO and TiO₂ nanoparticles at low contents on the crystallization, semicrystalline morphology, interfacial phenomena and segmental dynamics of PLA. *Mater. Today Commun.* **2021**, *27*, 102192–102202.
- (19) Yu, W.; Wang, X.; Ferraris, E.; Zhang, J. Melt crystallization of PLA/Talc in fused filament fabrication. *Mater. Des.* **2019**, *182*, 108013–108023.
- (20) Nofar, M.; Tabatabaei, A.; Park, C. B. Effects of nano-/micro-sized additives on the crystallization behaviors of PLA and PLA/CO₂ mixtures. *Polymer* **2013**, *54*, 2382–2391.
- (21) Han, L.; Pan, P.; Shan, G.; Bao, Y. Stereocomplex crystallization of high-molecular-weight poly(l-lactic acid)/poly(d-lactic acid) racemic blends promoted by a selective nucleator. *Polymer* **2015**, *63*, 144–153.
- (22) Lee, J. H.; Park, S. H.; Kim, S. H.; Ito, H. Replication and surface properties of micro injection molded PLA/MWCNT nanocomposites. *Polym. Test.* **2020**, *83*, 106321–106331.
- (23) Minelli, M.; Oradei, S.; Fiorini, M.; Sarti, G. C. CO₂ plasticization effect on glassy polymeric membranes. *Polymer* **2019**, *163*, 29–35.
- (24) Li, X.; Yang, D.; Zhao, Y.; Diao, X.; Bai, H.; Zhang, Q.; Fu, Q. Toward all stereocomplex-type polylactide with outstanding melt stability and crystallizability via solid-state transesterification between enantiomeric poly(l-lactide) and poly(d-lactide). *Polymer* **2020**, *205*, 122850–122860.
- (25) Qiao, Y.; Wang, Q.; Men, Y. Kinetics of Nucleation and Growth of Form II to I Polymorphic Transition in Polybutene-1 as Revealed by Stepwise Annealing. *Macromolecules* **2016**, *49*, 5126–5136.
- (26) Wang, H.-F.; Chiang, C.-H.; Hsu, W.-C.; Wen, T.; Chuang, W.-T.; Lotz, B.; Li, M.-C.; Ho, R.-M. Handedness of Twisted Lamella in Banded Spherulite of Chiral Polylactides and Their Blends. *Macromolecules* **2017**, *50*, 5466–5475.
- (27) Chrysafi, I.; Pavlidou, E.; Christodoulou, E.; Vourlias, G.; Klonos, P. A.; Kyritsis, A.; Bikiaris, D. N. Effects of poly(hexylene succinate) amount on the crystallization and molecular mobility of poly(lactic acid) copolymers. *Thermochim. Acta* **2021**, *698*, 178883–178893.
- (28) Li, Z.; Tan, B. H.; Lin, T.; He, C. Recent advances in stereocomplexation of enantiomeric PLA-based copolymers and applications. *Prog. Polym. Sci.* **2016**, *62*, 22–72.
- (29) Li, D.-c.; Liu, T.; Zhao, L.; Lian, X.-s.; Yuan, W.-k. Foaming of Poly(lactic acid) Based on Its Nonisothermal Crystallization Behavior under Compressed Carbon Dioxide. *Ind. Eng. Chem. Res.* **2011**, *50*, 1997–2007.
- (30) Liao, X.; Nawaby, A. V.; Whitfield, P. S. Carbon dioxide-induced crystallization in poly(L-lactic acid) and its effect on foam morphologies. *Polym. Int.* **2010**, *59*, 1709–1718.
- (31) Liu, W.; He, S.; Yang, Y. Effect of Stereocomplex Crystal on Foaming Behavior and Sintering of Poly(lactic acid) Bead Foams. *Polym. Int.* **2019**, *68*, 516–526.
- (32) Yan, Z.; Liao, X.; He, G.; Li, S.; Guo, F.; Li, G. Green Method to Widen the Foaming Processing Window of PLA by Introducing Stereocomplex Crystallites. *Ind. Eng. Chem. Res.* **2019**, *58*, 21466–21475.
- (33) Ren, Q.; Wang, J.; Zhai, W.; Su, S. Solid State Foaming of Poly(lactic acid) Blown with Compressed CO₂: Influences of Long Chain Branching and Induced Crystallization on Foam Expansion and Cell Morphology. *Ind. Eng. Chem. Res.* **2013**, *52*, 13411–13421.
- (34) Li, Y.; Mi, J.; Fu, H.; Zhou, H.; Wang, X. Nanocellular Foaming Behaviors of Chain-Extended Poly(lactic acid) Induced by Isothermal Crystallization. *ACS Omega* **2019**, *4*, 12512–12523.
- (35) Ji, G.; Zhai, W.; Lin, D.; Ren, Q.; Zheng, W.; Jung, D. W. Microcellular Foaming of Poly(lactic acid)/Silica Nanocomposites in Compressed CO₂: Critical Influence of Crystallite Size on Cell Morphology and Foam Expansion. *Ind. Eng. Chem. Res.* **2013**, *52*, 6390–6398.
- (36) Li, R.; Ye, L.; Zhao, X.; Coates, P.; Caton-Rose, F. Enhancing Poly(lactic acid) Microcellular Foams by Formation of Distinctive Crystalline Structures. *Ind. Eng. Chem. Res.* **2020**, *59*, 7624–7632.
- (37) Zhang, X.; Yang, B.; Fan, B.; Sun, H.; Zhang, H. Enhanced Nonisothermal Crystallization and Heat Resistance of Poly(l-lactic acid) by d-Sorbitol as a Homogeneous Nucleating Agent. *ACS Macro Lett.* **2021**, *10*, 154–160.
- (38) Pan, P.; Liang, Z.; Cao, A.; Inoue, Y. Layered Metal Phosphonate Reinforced Poly(l-lactide) Composites with a Highly Enhanced Crystallization Rate. *ACS Appl. Mater. Interfaces* **2009**, *1*, 402–411.
- (39) Tabatabaei, A.; Park, C. B. In-situ visualization of PLA crystallization and crystal effects on foaming in extrusion. *Eur. Polym. J.* **2017**, *96*, 505–519.
- (40) Liu, W.; Chen, P.; Wang, X.; Wang, F.; Wu, Y. Effects of Poly(butyleneadipate-co-terephthalate) as a Macromolecular Nucleat-

ing Agent on the Crystallization and Foaming Behavior of Biodegradable Poly(lactic acid). *Cell. Polym.* **2017**, *36*, 75–96.

(41) Lin, S.-H.; Wang, J.-M.; Wang, H.-T.; Wu, T.-M. Synthesis, mechanical properties and biodegradation of various acrylic acid-grafted poly(butylene succinate-co-terephthalate)/organically modified layered zinc phenylphosphonate nanocomposites. *Eur. Polym. J.* **2019**, *116*, 1–8.

(42) Chen, Y.; Qi, Y.; Tai, Z.; Yan, X.; Zhu, F.; Xue, Q. Preparation, mechanical properties and biocompatibility of graphene oxide/ultrahigh molecular weight polyethylene composites. *Eur. Polym. J.* **2012**, *48*, 1026–1033.

(43) Li, B.; Zhao, G.; Wang, G.; Zhang, L.; Gong, J. Fabrication of high-expansion microcellular PLA foams based on pre-isothermal cold crystallization and supercritical CO₂ foaming. *Polym. Degrad. Stab.* **2018**, *156*, 75–88.

(44) Ameli, A.; Jahani, D.; Nofar, M.; Jung, P. U.; Park, C. B. Development of high void fraction polylactide composite foams using injection molding: mechanical and thermal insulation properties. *Compos. Sci. Technol.* **2014**, *90*, 88–95.

(45) Najafi, N.; Heuzey, M.-C.; Carreau, P. J.; Therriault, D.; Park, C. B. Mechanical and morphological properties of injection molded linear and branched-poly(lactide (PLA) nanocomposite foams. *Eur. Polym. J.* **2015**, *73*, 455–465.

(46) Barmouz, M.; Behraves, A. H. Statistical and experimental investigation on low density microcellular foaming of PLA-TPU/cellulose nano-fiber bio-nanocomposites. *Polym. Test.* **2017**, *61*, 300–313.